

CONVOLUTIONAL NEURAL NETWORKS WITH A TOPOGRAPHIC REPRESENTATION MODULE FOR EEG-BASED BRAIN-COMPUTER INTERFACES

Xinbin Liang, National University of Defense Technology, Changsha, China, lxb2203@163.com

Yaru Liu, National University of Defense Technology, Changsha, China, lyrnudt@163.com

Yang Yu, National University of Defense Technology, Changsha, China, yuyangnurd@hotmai.com

Kaixuan Liu, National University of Defense Technology, Changsha, China, 2314825269@qq.com

Yadong Liu, National University of Defense Technology, Changsha, China, liuyadong1977@163.com

Zongtan Zhou, National University of Defense Technology, Changsha, China, narcz@163.com

Abstract

Objective: Convolutional Neural Networks (CNNs) have shown great potential in the field of Brain-Computer Interface (BCI) due to their ability to directly process the raw Electroencephalogram (EEG) without artificial feature extraction. The raw EEG signal is usually represented as 2-Dimensional (2-D) matrix composed of channels and time points, which ignores the spatial topological information of EEG. Our goal is to make the CNN with the raw EEG signal as input have the ability to learn the EEG spatial topological features, and improve its classification performance while essentially maintaining its original structure. Methods: We propose an EEG Topographic Representation Module (TRM). This module consists of (1) a mapping block from the raw EEG signal to a 3-D topographic map and (2) a convolution block from the topographic map to an output of the same size as the input. We embed the TRM to 3 widely used CNNs, and tested them on 2 different types of publicly available datasets. Results: The results show that the classification accuracies of the 3 CNNs are improved on both datasets after using TRM. The average classification accuracies of DeepConvNet, EEGNet and ShallowConvNet with TRM are improved by 4.70%, 1.29% and 0.91% on Emergency Braking During Simulated Driving Dataset (EBDSDD), and 2.83%, 2.17% and 2.00% on High Gamma Dataset (HGD), respectively. Significance: By using TRM to mine the spatial topological features of EEG, we improve the classification performance of 3 CNNs on 2 datasets. In addition, since the output of TRM has the same size as the input, any CNN with the raw EEG signal as input can use this module without changing the original structure.

Keywords: Convolutional Neural Network (CNN), Electroencephalogram (EEG), topographic representation, Brain-Computer Interface (BCI), EEG decoding, deep learning, ShallowConvNet, DeepConvNet, EEGNet.

1 Introduction

BCIs enable direct communication between human and machine via EEG (Wolpaw et al., 2002). EEG signal contains instinctive biometric information from the human brain. Through the precise EEG decoding, BCIs can recognize the user's inner thoughts. In general, the EEG decoding consists of 5 main stages: data collection, signal pre-processing, feature extraction, classification and data analysis (X. Zhang et al., 2020). Although these stages are essentially the same in a BCI paradigm, signal pre-processing (Bashashati et al., 2007), feature extraction (Mcfarland et al., 2006), and classification methods (Lotte et al., 2018) typically require substantial expertise and some prior knowledge about the BCI paradigm. Moreover, due to the manual processing, some useful information may be excluded from the extracted features, which poses a challenge to the subsequent classification and data analysis.

Deep learning has largely alleviated the need for manual feature extraction with the combination of feature extraction and classification. CNNs, in particular, have achieved great success in many challenging image classification tasks, outperforming approaches that rely on hand-crafted features (K. He et al., 2016; Hinton et al., 2012). Inspired by the success of deep learning in areas such as computer vision and natural language processing, researchers have introduced it to the EEG decoding area (Roy et al., 2019). CNNs are one of the most versatile deep learning methods in the BCI. Among all deep learning-based EEG decoding methods, those related to CNNs accounted for 53% of the total (43% for CNNs and 10% for hybrid-CNNs) (Craik, Y. He, and Contreras-Vidal, 2019). CNNs are typically composed of 3 structure blocks: convolutional layers, pooling layers and fully connected layers. The convolutional layer is an essential part of the CNN, which performs the feature extraction function. The pooling layer provides a down-sampling operation that both ensures learning of more robust features and reduces computation. The fully connected layer is typically located at the bottom of the network and implements the combined local features and classifier functions. The architecture of a CNN generally consists of layers arranged in a specific order, with earlier layers learning lower-level features and deeper layers learn high-level features. Several studies have use CNN models, including light (Bashivan et al., 2015; Lawhern et al., 2018; F. Li et al., 2020; M. Liu et al., 2018; Nicholas et al., n.d.; Schirrmeister et al., 2017) and deep (M. A. Li, Han, and Duan, 2019; Riyad, Khalil, and Adib, 2020; Schirrmeister et al., 2017; Tang, C. Li, and Sun, 2017) architectures, as well as other varieties (Alwasiti, Yusoff, and Raza, 2020; Dai et al., 2020; B. H. Lee, Jeong, and S. W. Lee, 2020; J. Li, Z. Zhang, and H. He, 2018; T. Liu and D. Yang, 2021; X. Liu et al., 2020; X. Zhu et al., 2019), to decode EEG signals. Waytowich et al. introduced a compact CNN for feature extraction and classification from the raw Steady-State Visually Evoked Potential (SSVEP) signal directly, with an average accuracy of about 80% cross-subject on a 12-class dataset (Nicholas et al., n.d.). By introducing batch normalization in the input and convolutional layers to cope with the overfitting problem, Liu et al. applied a CNN to the detection task of P300 signals, and achieved state-of-the-art recognition performance on both Dataset IIb of BCI competition II and Dataset II of BCI competition III (M. Liu et al., 2018). Tang et al. proposed a CNN model based on spatial-temporal features to classify single Motor Imagery (MI) tasks, and the results showed that compared with traditional methods, CNN can further improve classification performance (Tang, C. Li, and Sun, 2017). To address the overfitting problem of traditional machine learning methods in EEG-based emotion reading, Li et al. used a hierarchical CNN with differential entropy features from different channels as input, and achieved classification results with advantages compared to traditional methods (J. Li, Z. Zhang, and H. He, 2018). Li et al. proposed MI-VGG by modifying the VGG network to enable effective recognition of spectral images generated by MI-EEG and obtained competitive results on 3 publicly available datasets (M. A. Li, Han, and Duan, 2019).

EEG-based CNNs use both raw signals and features generated from raw signals as input. In this paper, we focus only on CNNs with the raw 2-D EEG signal as input. The raw EEG signal refers to the EEG data in the time domain, i.e., the $[C \text{ (Channels)} \times TP \text{ (Time Points)}]$ matrix. Since deep learning based CNN models have the ability to learn complex features from data without using hand-crafted features and can achieve end-to-end learning, the raw EEG signal is the most commonly used input formulation (Altaheri et al., 2021). Based on the classification error, CNNs learn and optimize the feature representation of the raw EEG signal simultaneously. Several competitive CNN models using raw EEG signals as input have been proposed (Amin et al., 2019; Dai et al., 2020; Fan et al., 2020; Jeong et al., 2020; Lawhern et al., 2018; D. Li et al., 2020; Schirrmeister et al., 2017; Tang, C. Li, and Sun, 2017; Wu et al., 2019; J. Yang et al., 2020). Schirrmeister et al. investigated more systematically the end-to-end learning from raw signals in EEG decoding using CNNs, and designed 2 widely used network architectures, DeepConvNet and ShallowConvNet (Schirrmeister et al., 2017). Test results on 2 different datasets showed that the proposed networks achieved at least as good classification performance as the best traditional methods. In addition, the visualization of the learned features also showed that the 2 networks performed an effective spatial mapping. Lawhern et al. introduced a compact CNN, EEGNet, which uses depth-wise and separable convolutions. Test results on 4 different types of BCI paradigms showed that EEGNet had better generalization ability, while obtaining comparable classification performance to others methods (Lawhern et al., 2018). Amin et al. used the raw EEG signal without preprocessing or artifact removal as input, and the classification performance was significantly improved by fusing multiple CNN models with different architectures (Amin et al., 2019). CNNs with the raw EEG signal as input, ignore the spatial inter-topology of the electrodes; therefore, most of these networks contain a spatial (depth) convolutional layer to learn the weights

of the electrodes, which is equivalent to a compensatory operation for ignoring the EEG spatial topological information.

In this paper, we introduce a Topographic Representation Module (TRM) to address the EEG spatial topological information loss problem caused by CNNs using raw EEG signals as input. The TRM consists of (1) a mapping block from the raw EEG signal to the topographic map and (2) a convolutional block transforming the topographic map into an output the same size as the input. That is, the size of the EEG signal will remain unchanged after passing through our TRM. Any CNN that takes the raw 2-D EEG signal as input can use this module. Such a design makes use of both the EEG spatial topological information and various existing excellent CNN architectures, making the TRM very versatile. The rest of this paper is organized as follows. Section 2 presents materials and methods, including datasets, classification algorithms, the TRM, implementation details and evaluation metrics. Section 3 presents the experimental results, i.e., algorithms performance under different evaluation metrics. Section 4 presents a discussion of the algorithms and the results. Finally, we give a conclusion.

2 MATERIALS AND METHODS

2.1 Datasets

The EEG signals in BCIs are generally classified into two types according to the presence or absence of external stimuli: evoked potentials and spontaneous EEG (X. Zhang et al., 2020). Evoked-potential BCIs have a clear external stimulus, and the EEG signal exhibits certain time-locked characteristics. Usually, this type of BCI has a high classification accuracy. Unlike evoked-potential BCIs, spontaneous EEG-based BCIs rely on the subject's spontaneous brain activity, usually without an external stimulus, and are generally more difficult to train. In this paper, we choose an evoked-potential BCI dataset and a spontaneous EEG-based BCI dataset, respectively.

Dataset 1: Emergency Braking During Simulated Driving Dataset (EBDSDD). EBDSDD has been described in detail in (Haufe et al., 2011). Here, we briefly describe it as follows. EBDSDD is a dataset of 2 types of tasks (emergency braking and non-braking) obtained from 18 subjects, each performing approximately 210 emergency braking (target) trials. EEG signals are recorded using 59 electrodes placed at the scalp sites, low-pass filtered at 45 Hz, and down-sampled to a sampling rate of 200 Hz. We refer to (Haufe et al., 2011) for the data processing method. The data from 1300 ms before emergency braking to 200 ms after braking are chosen as target segments. Non-target segments are normal driving EEG signals of length 1500 ms away from any stimulation and braking behavior for at least 3000 ms. Baseline correction is performed segment-wise using the data from the first 100 ms. For each subject, we choose the same number of the non-target segments and the target segments. In addition, Electrodes FP1, FP2, AF3 and AF4 are susceptible to the interference from the oculomotor potential, which we exclude and use only the remaining 55 electrodes. Therefore, the size of each target and non-target segment is 55 (channels) \times 280 (time points).

Dataset 2: High Gamma Dataset (HGD). HGD has been described in detail in (Schirrneister et al., 2017). Here, we give a brief description. HGD is a dataset of 4-class movements (left hand, right hand, feet and rest) obtained from 14 healthy subjects, each with approximately 1000 4-second trials of executed movements. The first approximately 880 trials are the training set and the last approximately 160 trials are the test set. HGD is a 128-electrode dataset with a sampling rate of 500 Hz. For the data processing method, we refer to (Schirrneister et al., 2017). 44 electrodes covering the motor cortex (all central electrodes except Cz, which is used as the recording reference electrode) are selected. The EEG signal is filtered using a 4-125 Hz bandpass filter and down-sampled to 250 Hz. We adopt the standard trial-wise training strategy, using the entire duration of the trial, so the matrix for each trial data is 44 (channels) \times 1000 (time points).

2.2 Classification Algorithms

In this paper, we use 3 widely used representative EEG-based CNNs: ShallowConvNet, DeepConvNet and EEGNet. They are CNNs specially designed for EEG decoding, and have shown better performance than traditional methods in many BCI applications.

ShallowConvNet. The design of ShallowConvNet is inspired by the Common Spatial Patterns of Filter Banks (FBCSP). It is similar to FBCSP in terms of EEG feature extraction. ShallowConvNet has a simple architecture, only consisting of a temporal convolution layer, a spatial convolution layer, an average pooling layer and a dense

layer. It has achieved better results than the best traditional methods in many EEG decoding tasks (Avilov et al., 2021; Gemein et al., 2020; Ingolfsson et al., 2020; Lawhern et al., 2018; Z. Liu et al., 2021; Riyad, Khalil, and Adib, 2020; Schirrmeister et al., 2017; L. Xu et al., 2021). For more details about ShallowConvNet, please refer to (Schirrmeister et al., 2017).

DeepConvNet. The architecture of DeepConvNet is inspired by the successful architecture of deep CNNs in computer vision, which aims to extract a wide range of features without relying on specific features types. DeepConvNet is designed as a general CNN architecture with the hope of achieving competitive accuracy with only a small amount of expert knowledge. It consists of four Conv-Pool blocks and a dense classification layer. The first Conv-Pool block is divided into a temporal convolutional layer, a spatial convolutional layer and a max-pooling layer. The other Conv-Pool blocks consist of only one convolutional layer and one max-pooling layer. DeepConvNet has achieved competitive classification accuracy compared to traditional methods in many EEG decoding tasks (Avilov et al., 2021; Gemein et al., 2020; Lawhern et al., 2018; Liang, 2020; Z. Liu et al., 2021; Riyad, Khalil, and Adib, 2020; Schirrmeister et al., 2017). For more details about DeepConvNet, please refer to (Schirrmeister et al., 2017).

EEGNet. EEGNet is designed to find a single CNN architecture that could be applied to different types of EEG-based BCIs, and make the network as compact as possible. The structure of EEGNet consists of 2 Conv-Pool blocks and a classification layer. In Block 1, it performs a temporal convolution and a depth-wise convolution sequentially. In Block 2, it uses separable convolution consisting of a depth-wise convolution and a point-wise convolution. In the classification layer, the SoftMax method is used. Due to the use of depth-wise and point-wise convolutions and the omission of the dense layer, this network design reduces the trainable parameters of EEGNet by at least an order of magnitude compared to other CNNs. Related studies have shown that EEGNet has a reasonable structure and excellent performance in different types of BCI paradigms (Avilov et al., 2021; Gemein et al., 2020; Ingolfsson et al., 2020; Kang; JiakaiZhang., 2022; Kostas and Rudzicz, 2020; Lawhern et al., 2018; Liang, 2020; Z. Liu et al., 2021; Riyad, Khalil, and Adib, 2020; Tsukahara et al., 2020; L. Xu et al., 2021; H. Zhao et al., 2020; Y. Zhu et al., 2021). For a detailed description of EEGNet, please refer to (Lawhern et al., 2018).

2.3 Topographic Representation Module

In order to make the CNN with the raw EEG signal as input more effective in utilizing the electrode spatial topological information, and to take full advantage of various existing excellent EEG-based CNNs, we introduce the EEG Topographic Representation Module (TRM). This module consists of (1) a mapping block from the raw EEG signal to the 3-D topographic map and (2) a convolution block from the topographic map to the processed output, as shown in Figure 1.

Mapping Block. According to the correspondence between the channels and electrode locations on the scalp, the raw EEG signal with the size of $[C(\text{channels}) \times TP(\text{time points})]$ is mapped into a 3-D EEG topographic map with the size of $[H(\text{height}) \times W(\text{width}) \times TP(\text{time points})]$. For the correspondence between the electrodes and the 2-D matrix coordinates of size $[H \times W]$, we refer to (Chao et al., 2019; Russo, 2021), and adjust the size of the matrix according to the distribution of electrodes. After mapping, the potential values of the raw EEG signal are kept constant, and for coordinates without corresponding electrodes on the matrix, we set them to 0. In this way, we transform the raw EEG signal into a 3-D topographic map represented by the electrode positions (matrix coordinates) and the corresponding potentials.

Convolution Block. We use convolution on the 3-D EEG topographic map to exploit its powerful feature learning capability. We make the output of the TRM the same size as the input so that the TRM could be embedded into these existing networks. C (channels) convolutional kernels of size (H, W) are used, and the 3-D EEG topographic map is convoluted to produce an output of size $[C \times TP]$. We choose a global convolution kernel with the same size as the 2-D matrix obtained from the mapping, because in the experiment, we find that it is better than using a combination of several local convolution kernels. After the convolutional layer, batch normalization is used to adjust the distribution of the data, and accelerate the training progress.

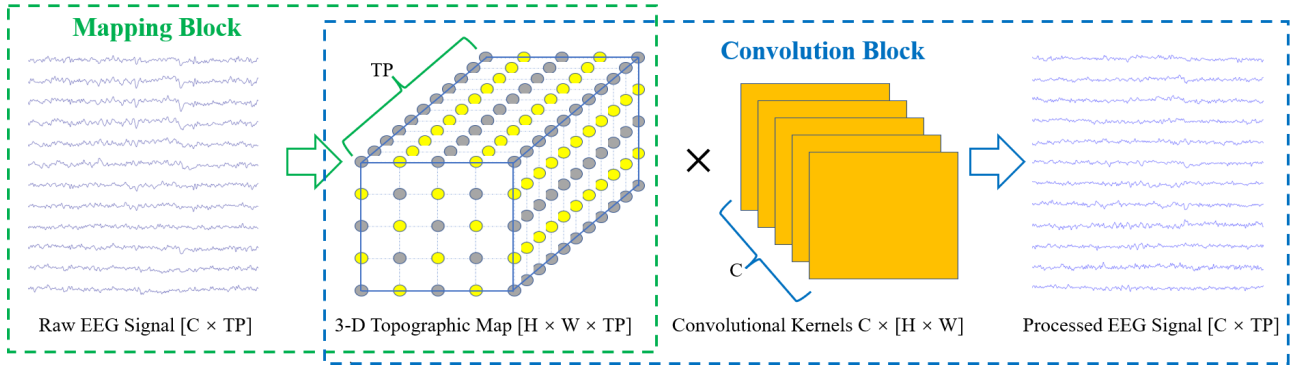


Figure 1: Overall visualization of EEG Topographic Representation Module (TRM). C: channels, TP: time points, H: height, W width. The parts framed by green and blue dashed lines are the mapping block and the convolution block, respectively. In the 3-D Topographic Map, coordinates of the yellow points correspond to the electrode locations of EEG, and the values are the potential values of the electrodes, while gray points have no corresponding electrodes and their values are set to 0. The output and input are of the same size.

2.4 Implementation Details

Figures 2 and 3 show the correspondence between electrode positions and matrix coordinates for EBDSD and HGD, respectively. The values of the yellow points in the matrix are the potential values of the corresponding electrodes, and the values of the gray points are set to 0. Each matrix is a 2-D EEG topographic map at a certain moment. By arranging the matrices in the temporal order of the EEG signal, a 3-D EEG topographic map is formed as shown in Figure 1. These 2 datasets were trained and tested for each subject using DeepConvNet, ShallowConvNet and EEGNet in their original form and with TRM, respectively. For EBDSD, we use a 4-fold cross-validation method, where 50% of the data from each subject is used as the training set, 25% as the validation set, and the remaining 25% as the test set. For HGD, the original data is split into a training set and a test set for each subject. We keep the test set unchanged, randomly select 80% of the original training set as the new training set, and the remaining 20% as the validation set. Each subject's data is trained and tested 4 times separately, and the average is taken as the final result. For a reasonable comparison, we set the same training and testing conditions for all 3 algorithms. For each algorithm, the settings are the same except for the use or non-use of TRM. All algorithms are trained and tested on a computer with an NVIDIA 2080-Ti graphics card. Several aspects of the algorithms are set up as follows.

- Adam optimizer is used with the weight-decay of 0.001, and the rest of the parameters are at default settings.
- Cross-entropy loss is used as a criterion.
- The batch size is set to 32.
- The training epoch is set to 300 and a validation stopping strategy is used. The algorithm's model with the lowest loss on the validation set is saved for testing.
- Both ShallowConvNet and EEGNet use the codes officially provided by braindecode for training and testing on both datasets (Schirrneister et al., 2017). On HGD, we use the code of DeepConvNet provided by the braindecode, while on EGDSD, we adjust DeepConvNet with the setting recommended by (Avilov et al., 2021) since the size of the input data do not meet the minimum length requirement of the original DeepConvNet.

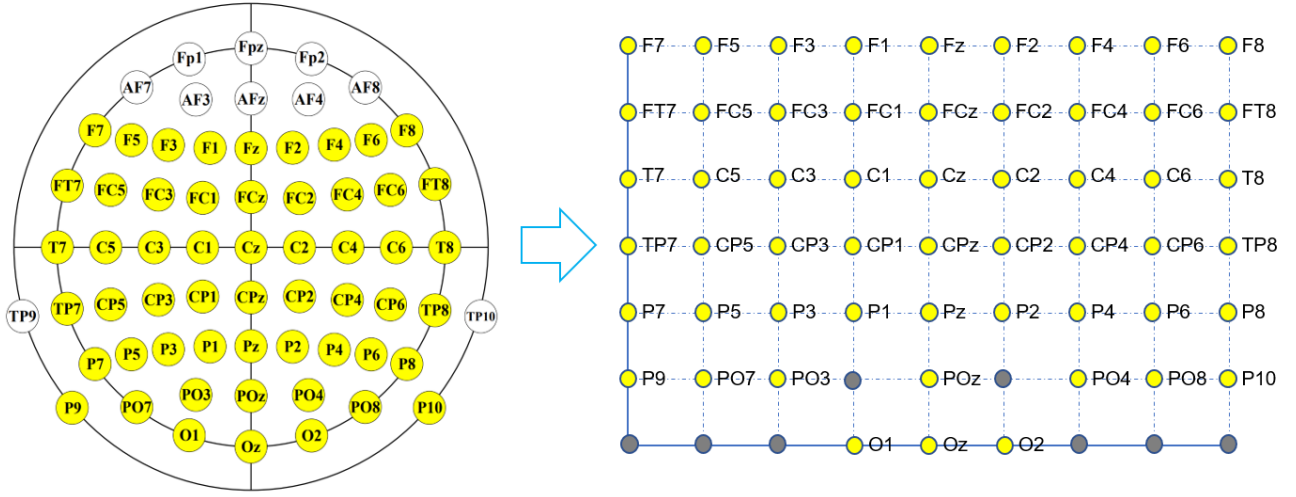


Figure 2: Correspondence between the electrode positions and the matrix coordinates on EBDSD. The value at the yellow point in the matrix is the potential value of the corresponding electrode, and the value of the gray point is set to 0. A total of 55 electrodes are used, and the size of the corresponding matrix is $[7 \times 9]$.

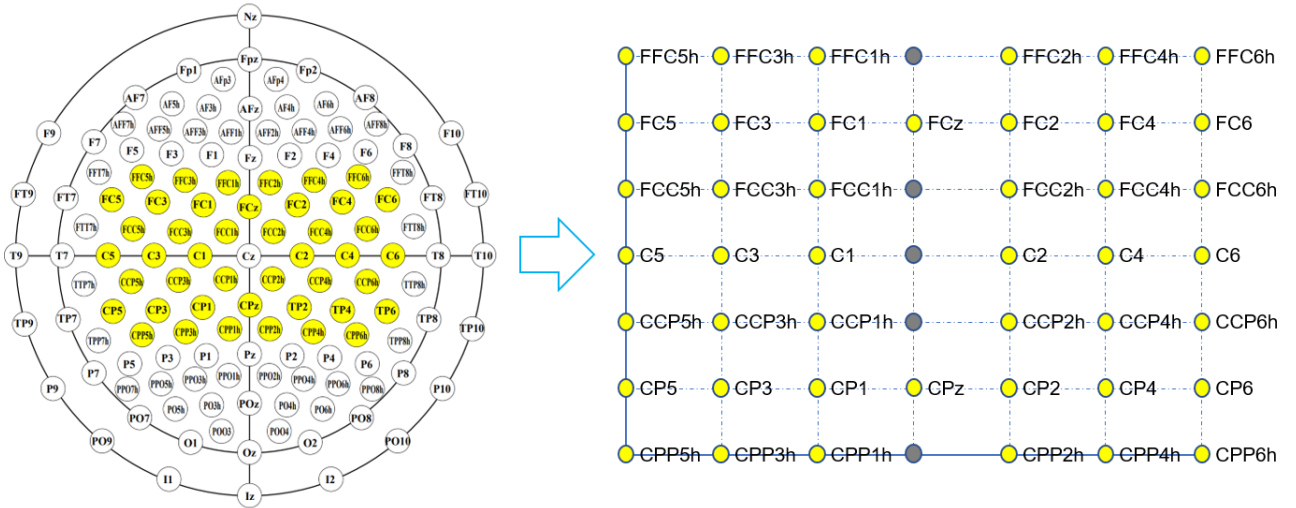


Figure 3: Correspondence between the electrode positions and the matrix coordinates on HGD. The values at the yellow point in the matrix is the potential value of the corresponding electrode, and the value of the gray point is set to 0. We use 44 electrodes covering the motor cortex (all central electrodes except Cz, which is using as the recording reference electrode), and the size of the corresponding matrix is $[7 \times 7]$.

2.5 Evaluation Metrics

We comprehensively compare the algorithms using metrics such as classification accuracy, training loss, validation loss, training epochs at lowest validation loss, and the time-consuming analysis. Classification accuracy refers to the ratio of the number of correct classifications to the total number. Training loss and validation loss are the cross-entropy loss of the algorithm on the training set and validation set, respectively. We also count the training epochs of different algorithms at the minimum validation loss. For the time-consuming analysis, we use

Table 1: Classification accuracies of 3 CNNs on EBDSD. The classification accuracy is expressed as the mean value \pm standard deviation of 4 test results, and the p-value is calculated by two-tailed paired t-test.

	DeepConvNet			EEGNet			ShallowConvNet		
Subject	Original	With TRM	Gain	Original	With TRM	Gain	Original	With TRM	Gain
VPae	77.99 \pm 1.86	80.98 \pm 5.43	2.99	88.86 \pm 2.99	93.75\pm3.25	4.89	88.32 \pm 3.25	88.04 \pm 2.94	-0.28
VPbad	90.77 \pm 4.56	91.22 \pm 1.13	0.45	95.95 \pm 3.93	97.07\pm1.35	1.12	96.40 \pm 1.80	95.72 \pm 1.86	-0.68
VPbax	84.43 \pm 5.18	85.96 \pm 6.83	1.53	89.91 \pm 2.32	90.79 \pm 2.32	0.88	92.54 \pm 1.83	94.52\pm1.10	1.98
VPbba	59.59 \pm 3.26	73.29 \pm 3.62	13.70	88.70 \pm 3.42	90.75\pm4.66	2.05	85.96 \pm 3.93	87.33 \pm 4.09	1.37
VPdx	81.44 \pm 6.44	87.87 \pm 0.95	6.43	91.83 \pm 1.49	94.06\pm1.40	2.23	90.35 \pm 6.88	89.60 \pm 4.61	-0.75
VPgaa	97.46 \pm 0.69	96.82 \pm 1.45	-0.64	98.31\pm1.55	97.88 \pm 1.09	-0.43	97.03 \pm 1.47	97.46 \pm 1.55	0.43
VPgab	89.12 \pm 2.55	91.44 \pm 3.96	2.32	94.21 \pm 1.17	95.83 \pm 0.93	1.62	96.76 \pm 1.93	96.99\pm1.39	0.23
VPgac	91.52 \pm 3.05	94.20 \pm 0.52	2.68	94.87 \pm 1.52	97.32\pm0.73	2.45	97.10 \pm 1.84	97.10 \pm 2.35	0
VPgae	84.21 \pm 4.18	87.94 \pm 2.90	3.73	91.67 \pm 2.53	94.08\pm0.44	2.41	87.50 \pm 4.66	87.28 \pm 4.21	-0.22
VPgag	86.76 \pm 5.69	93.63 \pm 2.47	6.87	96.57 \pm 2.47	97.30\pm2.02	0.73	96.08 \pm 1.39	96.08 \pm 0.80	0
VPgah	81.99 \pm 1.84	84.68 \pm 2.04	2.69	91.13 \pm 3.76	91.13 \pm 5.30	0	90.32 \pm 2.91	94.09\pm3.34	3.77
VPgal	77.97 \pm 2.96	86.39 \pm 6.07	8.42	94.31 \pm 3.99	92.57 \pm 4.16	-1.74	93.32 \pm 3.27	94.62\pm2.41	1.30
VPgam	81.19 \pm 4.42	88.57 \pm 1.35	7.38	92.14 \pm 2.95	93.10 \pm 1.96	0.96	90.71 \pm 1.63	94.76\pm1.23	4.05
VPih	78.30 \pm 8.95	87.03 \pm 4.83	8.73	95.52\pm2.09	95.05 \pm 2.09	-0.47	95.05 \pm 0.90	95.23 \pm 0.86	0.18
VPii	95.47 \pm 1.78	98.06 \pm 1.08	2.59	97.63 \pm 0.83	98.28 \pm 0.70	0.65	98.92\pm0.43	98.71 \pm 0.50	-0.21
VPja	90.53 \pm 6.70	93.45 \pm 3.66	2.92	94.42 \pm 1.66	94.9 \pm 1.22	0.48	95.63 \pm 2.31	95.87\pm1.46	0.24
VPsaj	89.58 \pm 4.56	96.30 \pm 1.51	6.72	96.99 \pm 0.89	97.22\pm1.07	0.23	94.91 \pm 3.82	97.22 \pm 2.00	2.31
VPsal	75.00 \pm 6.71	80.05 \pm 5.35	5.05	87.49 \pm 2.07	92.55\pm0.92	5.06	87.26 \pm 6.35	89.90 \pm 6.31	2.64
Average	84.07	88.77	4.70	93.36	94.65	1.29	93.01	93.92	0.91
p-value		2.92E-05			5.91E-3			1.82E-2	

300 epochs of the algorithm training and validation time.

3 RESULTS

3.1 Classification Accuracy

Accuracy On EBDSD. Table 1 shows the classification accuracies of 3 CNNs (ShallowConvNet, DeepConvNet and EEGNet) on EBDSD with and without TRM, respectively. Results for each subject are mean value \pm standard deviation of 4-fold cross-validation, and the p-value in the table is calculated by two-tailed paired t-test. For DeepConvNet, the classification accuracy of 17 subjects is improved after using ERM, with the highest increase of 13.70% (Subject VPbba), and only 1 subject has a slight decrease (Subject VPgaa with -0.64%). The average classification accuracy is improved by 4.70% (p-value < 0.001). For EEGNET, 14 subjects show an increase in classification accuracy with the highest increase of 5.06% (Subject VPsal) after using ERM, 3 subjects show a decrease (Subject VPgaa with -0.43%, Subject VPgal with -1.74%, and Subject VPih with -0.47%), and 1 subject (Subject VPgah) remains unchanged. The average classification accuracy is improved by 1.29% (p-value < 0.01). For ShallowConvNet, the classification accuracy increases in 11 subjects with a maximum of 4.05% (Subject VPgam), decreases in 5 subjects (Subject VPae with -0.28%, Subject VPbad with -0.68%, Subject VPdx with -0.75%, Subject VPgae with -0.22%, and Subject VPii with -0.21%) and remains unchanged in 2 subjects (Subject VPgac and Subject VPgag) after using ERM. The average result is improved by 0.91% (p-value < 0.05).

Accuracy On HGD. Table 2 shows the classification accuracies of the three CNNs on HGD with and without TRM, respectively. For DeepConvNet, classification accuracy increases in 12 subjects after using ERM, with the highest increase of 8.28% (Subject 5), and decreases in 2 subjects (Subject 2 with -1.10% and Subject 9 with -4.53%). The average classification accuracy increases by 2.83% (p-value < 0.05). For EEGNET, 12 subjects show an increase in classification accuracy after using ERM, with the highest increase of 7.19% (Subject 14) and 2 subjects show a decrease (Subject 1 with -1.56% and Subject 2 with -0.62%). The average classification

Table 2: Classification accuracies of 3 CNNs on HGD. The classification accuracy is expressed as the mean value \pm standard deviation of 4 test results, and the p-value is calculated by two-tailed paired t-test.

	DeepConvNet			EEGNet			ShallowConvNet		
Subject	Original	With TRM	Gain	Original	With TRM	Gain	Original	With TRM	Gain
1	54.06 \pm 3.63	56.41 \pm 5.04	2.35	62.34 \pm 1.64	60.78 \pm 6.28	-1.56	61.56 \pm 0.81	70.47\pm0.31	8.91
2	66.88 \pm 5.25	65.78 \pm 2.36	-1.10	70.00 \pm 2.55	69.38 \pm 3.02	-0.62	80.78\pm2.07	78.91 \pm 3.69	-1.87
3	83.13 \pm 6.02	89.84 \pm 2.90	6.71	93.13 \pm 3.61	94.06 \pm 1.57	0.93	94.84\pm1.39	94.06 \pm 1.08	-0.78
4	85.94 \pm 0.81	86.09 \pm 2.41	0.15	94.38 \pm 2.55	94.69 \pm 0.36	0.31	96.88 \pm 0.51	97.03\pm1.18	0.15
5	53.13 \pm 2.55	61.41 \pm 4.46	8.28	74.69 \pm 7.12	79.22 \pm 9.33	4.53	85.63\pm4.87	84.06 \pm 1.49	-1.57
6	58.75 \pm 3.95	61.56 \pm 4.96	2.81	83.91 \pm 2.62	85.16 \pm 2.19	1.25	88.13 \pm 2.10	88.75\pm1.35	0.62
7	59.84 \pm 3.55	63.13 \pm 2.65	3.29	66.09 \pm 7.76	67.34 \pm 9.85	1.25	75.31 \pm 1.65	80.94\pm2.19	5.63
8	73.59 \pm 2.30	73.75 \pm 3.10	0.16	76.25 \pm 3.78	80.47 \pm 4.69	4.22	84.22 \pm 1.80	87.50\pm3.89	3.28
9	64.22 \pm 6.20	59.69 \pm 3.13	-4.53	85.16 \pm 6.09	86.56\pm2.82	1.40	76.88 \pm 2.93	72.97 \pm 3.28	-3.91
10	78.59 \pm 3.48	81.88 \pm 4.11	3.29	84.53 \pm 1.64	85.94 \pm 3.00	1.41	85.94 \pm 3.40	86.88\pm3.78	0.94
11	65.78 \pm 2.25	68.28 \pm 3.55	2.50	79.69 \pm 9.58	84.22\pm7.58	4.53	77.66 \pm 5.14	82.50 \pm 5.03	4.84
12	79.22 \pm 6.09	81.56 \pm 3.25	2.34	83.13 \pm 2.55	87.19 \pm 2.42	4.06	88.75 \pm 1.14	90.16\pm1.72	1.41
13	60.94 \pm 4.16	68.91 \pm 7.47	7.97	77.50 \pm 3.42	78.91 \pm 0.60	1.41	78.75 \pm 5.80	86.56\pm1.08	7.81
14	69.69 \pm 8.67	75.16 \pm 5.46	5.47	77.50 \pm 5.89	84.69\pm5.56	7.19	70.16 \pm 3.24	72.66 \pm 5.65	2.50
Average	68.13	70.96	2.83	79.16	81.33	2.17	81.82	83.82	2.00
p-value		1.03E-02			4.83E-3			6.71E-2	

accuracy is improved by 2.17% (p-value < 0.01). For ShallowConvNet, the classification accuracy increases in 10 subjects with a maximum of 8.91% (Subject 1) and decreases in 4 subjects (Subject 2 with -1.87%, Subject 3 with -0.78, Subject 5 with -1.57, and Subject 9 with -3.91%) after using ERM. The average classification accuracy is improved by 2.00%.

3.2 Training Loss

Figure 4 shows the average training cross-entropy loss curves of the algorithms. Algorithms with “-TRM” mean that they use TRM. The left and right panels show the average training loss curves for 18 subjects on EBDSD and 14 subjects on HGD, respectively. On both datasets, DeepConvNet has the fastest decline in the training loss curve, followed by the ShallowConvNet, and the EEGNet is relatively flat. On EBDSD, the losses of all algorithms are relatively small after a period of training, which is related to the fact that this dataset is a 2-classification task with a high classification accuracy. We find that the training loss curves are not smooth, especially DeepConvNet and ShallowConvNet on HGD, which is related to the use of weight-decay to cope with the overfitting problem by imposing certain restrictions on the learning weights. The training loss of EEGNet is relatively gentle downward trend on both datasets, which we believe is related to the fact that it has fewer trainable parameters compared to the other two algorithms. After using TRM, the training loss curve of the algorithm follows roughly the same trend as the original algorithm.

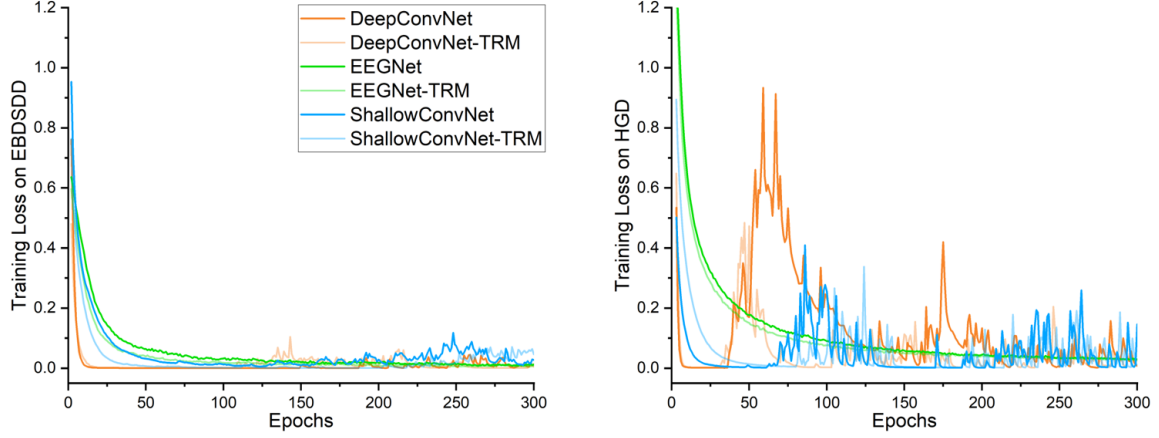


Figure 4: Training cross-entropy loss curves of different algorithms. The left and right panels show the average training loss curves of 18 subjects on EBDSD and 14 subjects on HGD, respectively. Algorithms with “-TRM” mean that they use TRM.

3.3 Validation Loss

Figure 5 shows the average validation loss curves of the algorithms. Algorithms with “-TRM” mean that they use TRM. The left and right panels show the average validation loss curves for 18 subjects on EBDSD and 14 subjects on HGD, respectively. Compared with the training loss curve, the validation curve provides a more accurate reflection of the classification and convergence performance of the algorithm. After the first few times of training, the verification loss of DeepConvNet is significantly higher than that of the other two algorithms on both datasets. On EBDSD, both EEGNet and ShallowConvNet have good validation loss curves, while on HGD, ShallowConvNet output performs EEGNet, which corresponds to the classification accuracy. Similar to what we see in the training loss curve, after using TRM, the validation loss curve basically follows the same trend as the original algorithm on both datasets. With TRM, the curves of all 3 algorithms show a downward trend, indicating that the TRM module is able to improve their classification performance.

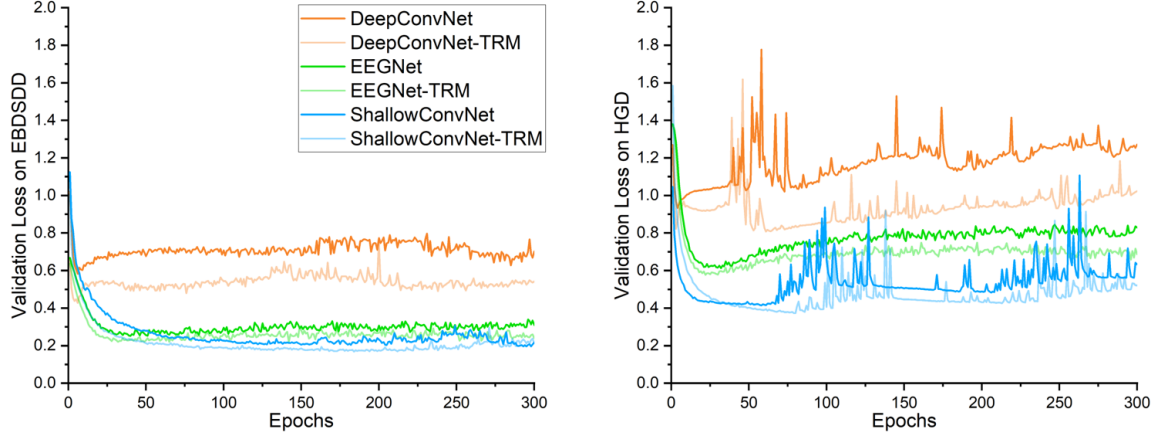


Figure 5: Validation cross-entropy loss curves of different algorithms. The left and right panels show the average validation loss curves of 18 subjects of EBDSD and 14 subjects of HGD, respectively.

3.4 Training Epochs at The Lowest Validation Loss

Figure 6 shows the average training epochs of the algorithms at the lowest validation loss. The left and right panels show the average training epochs for 18 subjects on EBDSD and 14 subjects on HGD, respectively. The average training epochs with the lowest validation loss on EBDSD is overall higher than that on HGD. With TRM, the average training epochs for DeepConvNet decreased and that for EEGNet increased on both datasets, while for ShallowConvNet, it is decreased on EBDSD and increased on HGD. The two-tailed paired t-test results show that the use of TRM has no significant effect on the average training epochs at the lowest validation loss.

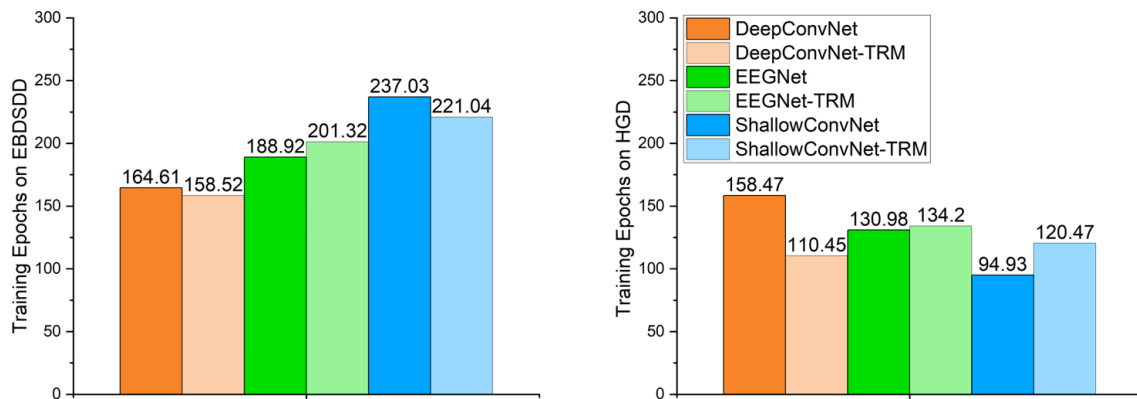


Figure 6: Average training epochs of the algorithms at the lowest validation loss. The left and right panels show the average training epochs of 18 subjects on EBDSD and 14 subjects on HGD, respectively.

3.5 Time Consumption Analysis

Considering the practicality in BCIs, we need to consider not only the classification accuracy, but also the execution time of the algorithm. Due to the addition of TRM, the execution time of the algorithm definitely increases. Figure Figure 7 shows the average time consumption of the algorithms for 300 training and validation epochs on each subject. The left and right panels show the average training time for 18 subjects on EBDSD and 14 subjects on HGD, respectively. On both datasets, ShallowConvNet consumes less time than DeepConvNet, and DeepConvNet consumes less time than EEGNet. After using TRM, the training and validation time of ShallowConvNet, DeepConvNet and EEGNet for 300 epochs increased by about 64%, 36%, 37% on EBDSD, and 34%, 23%, 17% on HGD, respectively. Meanwhile, we also find that ShallowConvNet-TRM consumes less time than DeepConvNet, and DeepConvNet-TRM consumes less time than EEGNet. The increased time consumption is relatively acceptable.

4 Discussion

The raw EEG signal is generally represented as a 2-D matrix form of $[C \text{ (channel)} \times TP \text{ (time points)}]$. In a CNN with the raw EEG signal as input, if there is no representation module about the electrode spatial topology in the network, the EEG signal will be processed as a tensor similar to a 2-D picture, and the spatial topological information of the electrode will be destroyed. The topographic map is a representation of the EEG signal as a 2-D or 3-D image, depending on the spatial topology of the electrodes (their positions on the scalp) (Altaheri et al., 2021). Topographic maps can be constructed using either the raw EEG signal (Liao et al., 2020; T. Liu and D. Yang, 2021; X. Zhao et al., 2019), or extracted features (Bashivan et al., 2015; Chao et al., 2019; Y. Li et al., 2017; Russo, 2021; M. Xu et al., 2020). If a CNN use the EEG topographic map constructed of the extracted feature as input, its performance depends on the quality of the extracted feature, which often requires substantial expertise and some prior knowledge. In studies of CNNs using topographic maps constructed from raw EEG signals as input, to the best of our current knowledge, all the networks have been designed according to the needs of tasks. Given that there are already many excellent CNNs with the input of raw EEG signal, it is possible to achieve the purpose of using spatial topological information of the EEG by simply adding a module without changing the structure of the original network.

Therefore, we designed the EEG Topographic Representation Module (TRM). By mapping the raw EEG signal into a 3-D topographic map, we make the input contain the spatial topological information of the electrodes. For those points that do not have electrodes corresponding to them, we adopted the practice of (X. Zhao

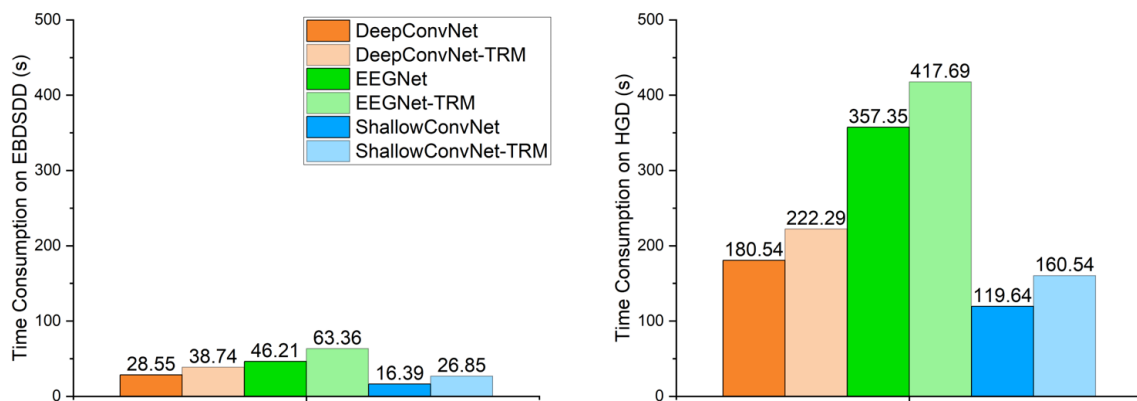


Figure 7: Average time consumption of the algorithms for 300 epochs training and validation epochs. The left and right panels show the average time consumption of 18 subjects on EBDSD and 14 subjects on HGD, respectively.

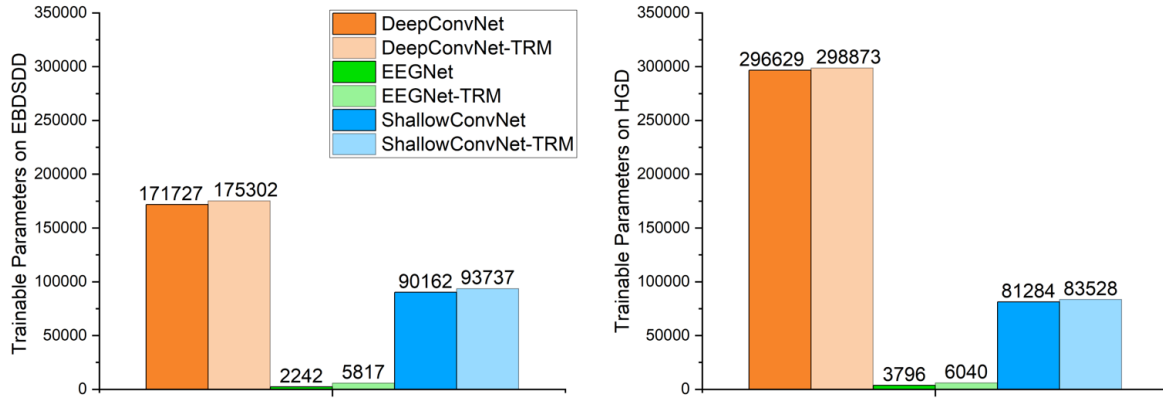


Figure 8: The number of trainable parameters of the algorithms. The left and right panels show the number of trainable parameters of the algorithms when trained on EBDSD and HGD, respectively.

et al., 2019) and set them directly to 0 instead of using interpolation, because in our experiments, we find that interpolation does not bring performance improvement, but increase the time consumption. We perform a convolution operation on the 3-D EEG topographic map to transform it into an output of the same dimension and size as the input. We choose a global spatial filter of the same size as the 2-D matrix obtained from the mapping, this is because in the experiments, we find that the global spatial filter works better than a combination of multiple local filters, a result consistent with (Liao et al., 2020). Such a design exploits both the powerful feature learning capabilities of deep learning and the ability to use various existing excellent CNNs in EEG-based BCIs.

We choose three widely used CNNs, ShallowConvNet with a shallow structure, DeepConvNet with a deep structure, and the compact EEGNet. And for datasets, we use two datasets from different types of BCI paradigms. It is hoped that these practices will make our results representative. We are very pleased to find that each CNN with TRM had a strong similarity to the original network, both in terms of the training loss curve and the validation loss curve, which indicates that the properties of the original CNNs are largely preserved after using TRM. Under the same training and test conditions and settings, the validation loss curves of 3 different CNNs all show a downward trend after using TRM on both datasets, which to some extent indicates that the TRM has the ability to improve the classification performance of EEG-based CNNs.

Since the size of the 3-D topographic map obtained by raw EEG signals is different, the number of trainable parameters of TRM will change accordingly. Figure 8 shows the number of trainable parameters of the 3 CNNs with or without TRM. The left and right panels show the number of trainable parameters of algorithms when trained on EBDSD and HGD, respectively. In our experiments, the number of TRM is 3575 when used on EBDSD and 2244 when used on HGD.

ShallowConvNet has a simple network structure, consisting of only a temporal convolution layer, a spatial convolution layer, a pooling layer and a dense layer, and the number of parameters is relatively moderate, so it has the fastest execution speed in all 3 CNNs. Even with TRM, it still consumes less time than DeepConvNet and EEGNet. On EBDSD, ShallowConvNet and ShallowConvNet-TRM achieve the best results on 7 out of 18 subjects. The average classification accuracy of ShallowConvNet is lower than that of EEGNet, while ShallowConvNet-TRM is higher than EEGNet, but still lower than EEGNet-TRM. On HGD, ShallowConvNet and ShallowConvNet-TRM achieve the best results on 11 out of 14 subjects, and the average classification accuracy is higher than other algorithms. Inspired by FBCSP, ShallowConvNet often has a better classification performance in spontaneous EEG decoding (Avilov et al., 2021; Lawhern et al., 2018). From the validation loss curve on HGD, we can also find that ShallowConvNet and ShallowConvNet-TRM have a smaller validation loss than other methods.

DeepConvNet has a deep structure and a large number of trainable parameters, which often requires a large

number of samples and uses certain skills to train it; therefore, it is more difficult to train and tends to be prone to overfitting when there are few samples (Avilov et al., 2021; Lawhern et al., 2018; Riyad, Khalil, and Adib, 2020). The classification results of DeepConvNet are poor on both datasets. And the validation loss curves also indicates that it has a larger validation loss compared to other methods. Although the classification accuracy of DeepConvNet increases after using TRM, it is still lower than ShallowConvNet and EEGNet. The time consumption of DeepConvNet is higher than that of ShallowConvNet. With TRM, its time consumption increases, but is still lower compared to EEGNet.

By the use of depth-wise and separable convolutions, and the omission of the dense layer, the number of trainable parameters in EEGNet is at least one order of magnitude smaller than the other two algorithms, which greatly alleviates the overfitting problem that often occurs in deep learning (Lawhern et al., 2018). Compared to the other two methods, EEGNet has a smoother training loss curve and validation loss curve. Although EEGNet has the least number of trainable parameters, it has a highest time consumption among the 3 CNNs. On EBDSD, EEGNet and EEGNet-TRM achieve the best results in 11 out of 18 subjects, and EEGNet-TRM accounts for 9 of them. Compared with EEGNet, the average classification accuracy of EEGNet-TRM is improved by 1.29% (p -value < 0.01), which is very valuable in such a high classification accuracy. On HGD, EEGNet and EEGNet-TRM achieve the best results of 3 out of 14 subjects, and all of them are obtained by EEGNet-TRM. The average classification accuracy of EEGNet with TRM is improved by 2.17% (p -value < 0.01), but it is still lower than that of ShallowConvNet.

By the analysis of the TRM structure, we find that most of the increased time is spent on mapping raw EEG signals into topographic maps, while the one-layer convolution block consumes very little time. If EEG signal is collected in the form of 3-D matrix (3-D topographic map), the TRM can omit the mapping process. In this case, we find that the additional time consumption is almost negligible compared to the original algorithm.

5 Conclusion

In this paper, we introduce an EEG Topographic Representation Module (TRM). This module consists of a mapping block and a convolution block, and has an output the same size as its input. Any CNN with the raw EEG signal as input can use TRM. We selected 3 representative CNNs and tested them on 2 different types of BCI datasets. Results show that the classification accuracy of all 3 algorithms is improved after using TRM. Next, we intend to train and test TRM on more CNNs and more datasets for a further validation. In addition, we want to improve the TRM structure to reduce its time consumption.

References

- Altaheri, Hamdi, Ghulam Muhammad, Mansour Alsulaiman, Syed Umar Amin, Ghadir Ali Altuwaijri, Wadood Abdul, Mohamed A. Bencherif, and Mohammed Faisal (2021). “Deep learning techniques for classification of electroencephalogram (EEG) motor imagery (MI) signals: a review.” *Neural Computing and Applications*, 1–42.
- Alwasiti, H., M. Z. Yusoff, and K. Raza (2020). “Motor Imagery Classification for Brain Computer Interface Using Deep Metric Learning.” *IEEE Access* 8, 109949–109963.
- Amin, S. U., M. Alsulaiman, G. Muhammad, Mam Amine, and M. S. Hossain (2019). “Deep Learning for EEG motor imagery classification based on multi-layer CNNs feature fusion.” *Future Generation Computer Systems* 101.
- Avilov, O., S. Rimbert, A. Popov, and L. Bougrain (2021). “Optimizing Motor Intention Detection With Deep Learning: Towards Management Of Intraoperative Awareness.” *IEEE Transactions on Biomedical Engineering* PP (99), 1–1.
- Bashashati, Ali, Mehrdad Fatourehchi, Rabab K Ward, and Gary E Birch (2007). “A survey of signal processing algorithms in brain-computer interfaces based on electrical brain signals.” *Journal of Neural Engineering* 4 (2), R32.
- Bashivan, P., I. Rish, M. Yeasin, and N. Codella (2015). “Learning Representations from EEG with Deep Recurrent-Convolutional Neural Networks.” *Computer ence*.
- Chao, H., L. Dong, Y. Liu, and B. Lu (2019). “Emotion Recognition from Multiband EEG Signals Using CapsNet.” *Sensors* 19 (9), 2212.
- Craik, A., Y. He, and Jose Luis Contreras-Vidal (2019). “Deep Learning for Electroencephalogram (EEG) Classification Tasks: A Review.” *Journal of Neural Engineering*.
- Dai, G., J. Zhou, J. Huang, and N. Wang (2020). “HS-CNN: a CNN with hybrid convolution scale for EEG motor imagery classification.” *Journal of neural engineering* 17 (1), 016025.1–016025.11.
- Fan, Chen Chen, Hongjun Yang, Zeng Guang Hou, Zhen Liang Ni, and Zhi Jie Fang (2020). “Bilinear neural network with 3-D attention for brain decoding of motor imagery movements from the human EEG.” *Cognitive Neurodynamics* (1).
- Gemein, Law, R. T. Schirrmester, P. Chrabszcz, D. Wilson, and T. Ball (2020). “Machine-Learning-Based Diagnostics of EEG Pathology.” *NeuroImage* 220.
- Haufe, Stefan, Matthias S Treder, Manfred F Gugler, Max Sagebaum, Gabriel Curio, and Benjamin Blankertz (2011). “EEG potentials predict upcoming emergency brakings during simulated driving.” *Journal of Neural Engineering* (No.10), 056001–056013.
- He, K., X. Zhang, S. Ren, and J. Sun (2016). “Deep Residual Learning for Image Recognition.” *IEEE*.
- Hinton, G., L. Deng, D. Yu, G. E. Dahl, and B. Kingsbury (2012). “Deep Neural Networks for Acoustic Modeling in Speech Recognition: The Shared Views of Four Research Groups.” *IEEE Signal Processing Magazine* 29 (6), 82–97.
- Ingolfsson, T. M., M. Hersche, X. Wang, N. Kobayashi, and L. Benini (2020). “EEG-TCNet: An Accurate Temporal Convolutional Network for Embedded Motor-Imagery Brain-Machine Interfaces.”
- Jeong, J. H., B. H. Lee, D. H. Lee, Y. D. Yun, and S. W. Leeb (2020). “EEG Classification of Forearm Movement Imagery Using A Hierarchical Flow Convolutional Neural Network.” *IEEE Access* PP (99), 1–1.
- Kang;JiacaiZhang., Ran Shi;Yanyu Zhao;Zhiyuan Cao;Chunyu Liu;Yi (2022). “Categorizing objects from MEG signals using EEGNet.” *Cognitive Neurodynamics* (No.2), 365–377 (No.2).
- Kostas, D. and F. Rudzicz (2020). “Thinker invariance: enabling deep neural networks for BCI across more people.” *Journal of Neural Engineering* 17 (5), 056008 (22pp).
- Lawhern, Vernon J, Amelia J Solon, Nicholas R Waytowich, Stephen M Gordon, Chou P Hung, and Brent J Lance (2018). “EEGNet: A Compact Convolutional Network for EEG-based Brain-Computer Interfaces.” *Journal of Neural Engineering* 15 (5), 056013.1–056013.17.
- Lee, B. H., J. H. Jeong, and S. W. Lee (2020). “SessionNet: Feature Similarity-based Weighted Ensemble Learning for Motor Imagery Classification.” *IEEE Access* PP (99), 1–1.

- Li, D., J. Xu, J. Wang, X. Fang, and J. Ying (2020). "A Multi-Scale Fusion Convolutional Neural Network Based on Attention Mechanism for the Visualization Analysis of EEG Signals Decoding." *IEEE Transactions on Neural Systems and Rehabilitation Engineering* PP (99), 1–1.
- Li, Feng, Fan He, Huiguang He, Fei Wang, Dengyong Zhang, Yi Xia, and Xiaoyu Li (2020). "A Novel Simplified Convolutional Neural Network Classification Algorithm of Motor Imagery EEG Signals Based on Deep Learning." *Applied Sciences* (No.5), 1605.
- Li, Jinpeng, Zhaoxiang Zhang, and Huiguang He (2018). "Hierarchical Convolutional Neural Networks for EEG-Based Emotion Recognition." *Cognitive Computation* (No.2), 368–380.
- Li, M. A., J. F. Han, and L. J. Duan (2019). "A Novel MI-EEG Imaging With the Location Information of Electrodes." *IEEE Access* PP (99), 1–1.
- Li, Youjun, Jiajin Huang, Haiyan Zhou, and Ning Zhong (2017). "Human Emotion Recognition with Electroencephalographic Multidimensional Features by Hybrid Deep Neural Networks." *Applied Sciences* (No.10), 1060.
- Liang, Dongxu Yang;Yadong Liu;Zongtan Zhou;Yang Yu;Xinbin (2020). "Decoding Visual Motions from EEG Using Attention-Based RNN." *Applied Sciences* (No.5662), 5662 (No.5662).
- Liao, Jacob Jiexun, Joy Jiayu Luo, Tao Yang, Rosa Qi Yue So, and Matthew Chin Heng Chua (2020). "Effects of local and global spatial patterns in EEG motor-imagery classification using convolutional neural network." *Brain-Computer Interfaces* (1), 1–10.
- Liu, M., W. Wu, Z. Gu, Z. Yu, F. F. Qi, and Y. Li (2018). "Deep learning based on Batch Normalization for P300 signal detection." *Neurocomputing* 275 (JAN.31), 288–297.
- Liu, T. and D. Yang (2021). "A Densely Connected Multi-Branch 3D Convolutional Neural Network for Motor Imagery EEG Decoding." *Brain Sciences* 11 (2), 197.
- Liu, X., Y. Shen, J. Liu, J. Yang, and F. Lin (2020). "Parallel Spatial–Temporal Self-Attention CNN-Based Motor Imagery Classification for BCI." *Frontiers in Neuroscience* 14.
- Liu, Z., L. Meng, X. Zhang, W. Fang, and D. Wu (2021). "Universal adversarial perturbations for CNN classifiers in EEG-based BCIs." *Journal of Neural Engineering* 18 (4), 0460a4 (16pp).
- Lotte, F., Bougrain, L., Cichocki, A., Clerc, M., Congedo, and Rakotomamonjy (2018). "A review of classification algorithms for EEG-based brain-computer interfaces: a 10 year update." *Journal of neural engineering*.
- Mcfarland, D. J, C. W. Anderson, K. R Muller, A Schlogl, and D. J. Krusienski (2006). "BCI meeting 2005-workshop on BCI signal processing: feature extraction and translation." *IEEE Trans Neural Syst Rehabil Eng* 14 (2), 135–138.
- Nicholas, W., V. J. Lawhern, J. O. Garcia, C. Jennifer, F. Josef, S. Paul, and J. M. Vettel (n.d.). "Compact convolutional neural networks for classification of asynchronous steady-state visual evoked potentials." *Journal of neural engineering* () ()
- Riyad, M., M. Khalil, and A. Adib (2020). "MI-EEGNET: A novel Convolutional Neural Network for motor imagery classification." *Journal of Neuroscience Methods* 353, 109037.
- Roy, Y., H. Banville, I. Albuquerque, A. Gramfort, and J. Faubert (2019). "Deep learning-based electroencephalography analysis: a systematic review." *Journal of Neural Engineering*.
- Russo, Ante Topic;Mladen (2021). "Emotion recognition based on EEG feature maps through deep learning network." *Engineering Science and Technology, an International Journal* (No.6), 1442–1454 (No.6).
- Schirrmeister, R. T., J. T. Springenberg, Ldj Fiederer, M. Glasstetter, K. Eggenberger, M. Tangermann, F. Hutter, W. Burgard, and T. Ball (2017). "Deep learning with convolutional neural networks for EEG decoding and visualization."
- Tang, Z., C. Li, and S. Sun (2017). "Single-trial EEG classification of motor imagery using deep convolutional neural networks." *Optik - International Journal for Light and Electron Optics*.
- Tsukahara, Akihiko, Yuki Anzai, Keita Tanaka, and Yoshinori Uchikawa (2020). "A design of EEGNet-based inference processor for pattern recognition of EEG using FPGA." *Electronics and Communications in Japan*.
- Wolpaw, Jonathan R, Niels Birbaumer, Dennis J McFarland, Gert Pfurtscheller, and Theresa M Vaughan (2002). "Brain–computer interfaces for communication and control." *Clinical Neurophysiology*.
- Wu, H., Y. Niu, F. Li, Y. Li, and M. Dong (2019). "A Parallel Multiscale Filter Bank Convolutional Neural Networks for Motor Imagery EEG Classification." *Frontiers in Neuroscience* 13.

- Xu, L., M. Xu, Z. Ma, K. Wang, T. P. Jung, and D. Ming (2021). “Enhancing transfer performance across datasets for brain-computer interfaces using a combination of alignment strategies and adaptive batch normalization.” *Journal of neural engineering* 18 (4).
- Xu, M., J. Yao, Z. Zhang, R. Li, and J. Zhang (2020). “Learning EEG Topographical Representation for Classification via Convolutional Neural Network.” *Pattern Recognition* 105 (4), 107390.
- Yang, J., Z. Ma, J. Wang, and Y. Fu (2020). “A Novel Deep Learning Scheme for Motor Imagery EEG Decoding Based on Spatial Representation Fusion.” *IEEE Access* 8, 202100–202110.
- Zhang, X., L. Yao, X. Wang, Jjm Monaghan, and Y. Zhang (2020). “A survey on deep learning-based non-invasive brain signals: recent advances and new frontiers.” *Journal of Neural Engineering*.
- Zhao, Haifeng, Yikai Yang, Petra Karlsson, and Alistair Mcewan (2020). “Can recurrent neural network enhanced EEGNet improve the accuracy of ERP classification task? An exploration and a discussion.” *Health and Technology* 10 (4), 979–995.
- Zhao, X., H. Zhang, G. Zhu, F. You, S. Kuang, and L. Sun (2019). “A Multi-Branch 3D Convolutional Neural Network for EEG-Based Motor Imagery Classification.” *IEEE transactions on neural systems and rehabilitation engineering* 27 (10), 2164–2177.
- Zhu, X., P. Li, C. Li, D. Yao, R. Zhang, and P. Xu (2019). “Separated channel convolutional neural network to realize the training free motor imagery BCI systems.” *Biomedical Signal Processing and Control* 49 (MAR.), 396–403.
- Zhu, Y., Y. Li, J. Lu, and P. Li (2021). “EEGNet With Ensemble Learning to Improve the Cross-Session Classification of SSVEP Based BCI From Ear-EEG.” *IEEE Access* 9, 15295–15303.